CrossMark

Nitrogen-doped carbon enhanced mesoporous TiO$_2$ in photocatalytic remediation of organic pollutants

Dian Li[1] · Yupu Liu[2] · Hong Liu[1] · Zhihua Li[1] · Li Lu[1] · Jun Liang[1] · Zhonghui Huang[1] · Wei Li[2] ⓘ

Abstract

Controllable synthesis of mesoporous photocatalysts is of great interest for the photocatalytic remediation of organic pollutants from wastewater by sunlight. In this work, we have developed a new photocatalyst with nitrogen-doped carbon (NC) and mesoporous TiO$_2$ (mTiO$_2$) interpenetrating hetero-structure by a sol–gel process combined with an in situ carbonization strategy. The synthesized nanospheres possess a uniform particle size ($\sim$ 60 nm), high surface area ($\sim$ 108 m^2/g), and large pore diameter ($\sim$ 2.1 nm). Most importantly, the nanospheres consist of ultrasmall TiO$_2$ nanocrystals ($\sim$ 8.2 nm), which are uniformly coated by a thin layer of N-doped carbon. Significantly, the resultant NC/mTiO$_2$ composite nanospheres exhibit a broad light absorption in the range of 200–2000 nm (entire wavelength). When serving as a photocatalyst for organic pollutants degradation, high performance was obtained. Accordingly, the resultant NC/mTiO$_2$ composite nanospheres performed in an excellent manner in the photodegradation of methyl orange, and the total removal efficiency was up to 97.7%, much better than that of commercial P25 (19.8%). Furthermore, the nanocomposite also effectively photodegraded other organic pollutants such as methylene blue (dyestuff) and phenol, respectively. Therefore, the resultant NC/mTiO$_2$ nanocomposites have potential applications in environmental cleanup.

Keywords Mesoporous materials · TiO$_2$ · Composites · Photocatalysis · Organic pollutants

---

Dian Li and Yupu Liu contributed equally to this work.

✉ Wei Li
weilichem@fudan.edu.cn

Extended author information available on the last page of the article

Introduction

Wastewater derived from chemical industries such as petrochemical, pesticide, pigment, dyestuff, and papermaking usually has high concentrations of organic dyes, phenol and its derivatives, which are notorious in recent years because of their environmental and health impacts [1–4]. Several traditional methods, such as filtration, adsorption, selective precipitation, and chemical oxidation are currently worked for the elimination of these pollutants from the natural environment [5–8]. However, these methods can not totally decompose them, but bring other shortcomings (i.e., a time-consuming process, high-cost, and secondary pollution) [7, 8]. In contrast, heterogeneous photocatalysis is simple, low cost, and can be adopted on a wide scale [9, 10]. Therefore, the study of the organic pollutants photodegradation has become increasingly popular [11, 12].

Among various photocatalysts, mesoporous TiO_2 ($mTiO_2$) have attracted a great deal of attention in the past decade caused by their outstanding advantages such as large pore diameter, high surface area, low cost, nontoxicity, perfect chemical and thermal stability [13–16]. The mesoporous structure can provide more active sites with much higher accessibility during the catalytic process, thus favoring the molecules diffusion compared to bulk counterparts [13–17]. However, considering the high band gap of TiO_2 ($\sim$ 3.2 eV), only $\sim$ 5% of sunlight can be used. At the same time, the photogenerated electron–hole pair is easy to recombine, thus leading to low quantum efficiency [18, 19]. These problems severely hinder their large-scale applications for organic pollutants degradation.

Carbon-based materials with many interesting physical and chemical properties have been extensively explored to be a superlative conductive substrate to increase TiO_2 photocatalytic performance [20–22]. Both theoretical and experimental studies have displayed that nitrogen doping provides an effective approach to tailor the electronic property and chemical reactivity of carbon materials. Thus, nitrogen-doped carbon (NC) materials, as a novel derivative, show high-performance as an electron cocatalyst of photocatalysts relative to pristine carbon-based materials [23–25]. Moreover, the stronger hydrophobic or/and π–π stacking interactions between NC materials and organic pollutants is favorable for the adsorption of organic molecules. For example, Liu et al. have prepared nitrogen-doped graphene/TiO_2 nanocomposites, which appeared to be excellent visible light photocatalysts for photodegradation of eosin Y [26]. Ding et al. [27] have developed nitrogen–doped GO/TiO_2 membranes with an enhanced photocatalytic performance and superior anti-fouling properties. So far, most of studies have been concentrated on the preparation of N-doped graphene-based/TiO_2 composites [21–29]. However, the addition of graphene-based materials may also bring high-cost, complex and time-consuming processes. Therefore, it is still of great important to develop a low-cost and facile method for preparing new nitrogen-doped carbon-based materials/TiO_2 composites, which could meet the requirements for efficient photodegradation of organic pollutants.

In this work, we demonstrate the preparation of N-doped carbon/mesoporous TiO_2 ($NC/mTiO_2$) composite nanospheres by a sol–gel process combined with an

in situ carbonization strategy. The resultant composite nanospheres possess a uniform particle size ($\sim$ 60 nm), high surface area ($\sim$ 108 m^2/g), and large pore diameter ($\sim$ 2.1 nm). Moreover, the nanospheres consist of ultrasmall TiO$_2$ nanocrystals ($\sim$ 8.2 nm), which are uniformly coated by a thin layer of N-doped carbon. This synthesis method is simple, convenient, inexpensive, and can be easily reproduced on a large-scale. Importantly, the resultant NC/mTiO$_2$ composite nanospheres show excellent photocatalytic activity for dyes and phenol photodegradation under UV–Vis light irradiation, which is much higher than commercial TiO$_2$ powders (P25). It is mainly attributed to the admirable light absorption in the range from 200 to 2000 nm. We believe this study offers a new notion for the synthesis of TiO$_2$-based nanomaterials as high-performance photocatalysts.

Experimental section

Preparation of NC/mTiO$_2$ composite nanospheres

First, amorphous TiO$_2$ nanospheres were achieved via a sol–gel method. Typically, 0.4 g HDA and 0.8 g P123 were dissolved in 60 g ethanol. Later, 7.5 g H$_2$O was added. Then, 0.48 mL TBOT was dropped into the solution with stirring. The white precipitate formed under static stirring for 12 h. NC/mTiO$_2$ was obtained by calcination of the white precipitate in N$_2$ at 750 °C for 4 h.

Photodegradation measurements

The photoactivities of the resultant composites were investigated by the photocatalytic remediation of methyl orange, methylene blue, and phenol under UV–Vis light irradiation. In a typical experiment, 25 mg of the composites were added into a flask containing 50 mL of organic pollutant solution (80 mg/L), and then the mixed solution was shaken in the dark overnight. Next, the mixture was irradiated under a 350 W Xenon lamp. Time-dependent measurements checking the activities were carried out by using a JASCO V-550 spectrophotometer. As a control, commercial P25 were also tested under the same conditions.

Measurements and characterization

Nitrogen sorption isotherms were measured at 77 K with a Micromeritcs Tristar 2420 analyzer. The Brunauer–Emmett–Teller (BET) method was used to evaluate the specific surface area using adsorption data in a relative pressure range from 0.05 to 0.25 with $R > 0.995$. Using the Barrett–Joyner–Halenda (BJH) model, the pore volume and pore size distribution were derived from the adsorption branch of isotherms, and the total pore volume (V_t) was estimated from the adsorbed amount at a relative pressure P/P_0 of 0.995. The diffuse reflection spectra were collected on a Shimadzu UV-2450 spectrophotometer (Japan) using BaSO$_4$ as a reference. Transmission electron microscopy (TEM) experiments were conducted on a JEOL JEM–2100 F microscope (Japan) operated at 200 kV. Field–emission scanning

electron microscopy (FESEM) images were taken on a Hitachi S–4800 microscope. Thermogravimetric analysis was conducted on a Mettler Toledo TGA-SDTA851 analyzer (Switzerland) from 30 to 900 °C under oxygen with a heating rate of 5 °C/min. Wide-angle X-ray diffraction (XRD) patterns were recorded on a Bruker D8 diffractometer (Germany) with Ni-filtered Cu Kα radiation (40 kV, 40 mA). X-ray photoelectron spectroscopy (XPS) experiments were carried out on a RBD upgraded PHI-5000C ESCA system (Perkin Elmer) with Mg Kα radiation (hv = 1253.6 eV).

Results and discussion

As revealed by FESEM and TEM images, TiO_2 colloidal nanospheres were first prepared through a sol–gel method with a diameter of $\sim$ 90 nm (Figure S1). Since there are the hydrophilic or/and electrostatic interactions between the titanium oligomers and hydrophilic segments of surfactants (P123 and HDA) [30, 31], the resultant TiO_2 colloidal nanosphere is a hybrid structure, consisting of an amorphous TiO_2 matrix and organic templates. After annealing under a nitrogen atmosphere, the development of NC framework throughout the highly crystallized TiO_2 matrix was demonstrated by the color transform to gray (Figure S2). The SEM
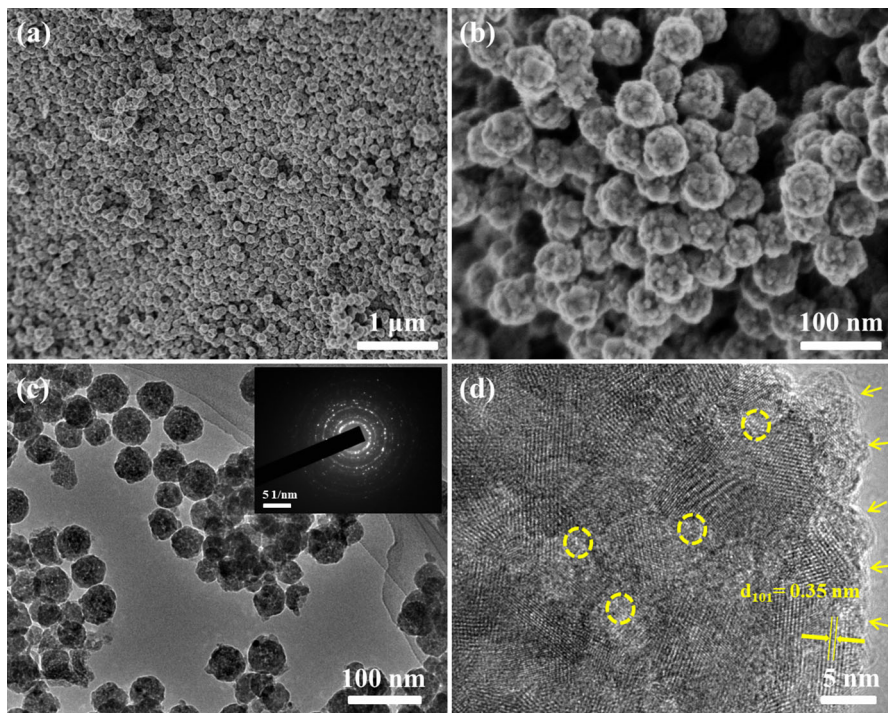

Fig. 1 **a**, **b** SEM and **c** TEM images of the NC/mTiO$_2$ composite nanospheres prepared via a sol–gel process followed by sequential carbonization of surfactants. The inset in **c** is the SAED pattern of the NC/mTiO$_2$ composite nanospheres. **d** HRTEM image of a NC/mTiO$_2$ composite nanosphere

image (Fig. 1a) of the resultant NC/mTiO$_2$ composite nanospheres shows obvious monodispersed features with a particle size of $\sim$ 60 nm. Simultaneously, the SEM image (Fig. 1b) also reveals a wormhole-like mesoporous structure. A TEM image displays all the nanospheres consisting of ultrasmall TiO$_2$ particles (Fig. 1c) and a highly mesoporous structure with a pore size of $\sim$ 2.5 nm. The high resolution TEM (HRTEM) image clearly displays that the samples are well crystallized with the d-spacing of $\sim$ 0.35 nm matched to the d_{101} lattice of anatase TiO$_2$. The well-defined mesopores have been highlighted by cycles in Fig. 1d. The selected-area electron diffraction (SAED) pattern (Fig. 1c, inset) further discloses the polycrystalline feature of anatase TiO$_2$. In addition, the thin amorphous carbon sheets could be clearly detected around highly crystallized TiO$_2$ nanoparticles, as denoted by the arrows (Fig. 1d). The scanning transmission electron microscopy (STEM) image reveals that NC/mTiO$_2$ composite nanosphere is highly porous (Fig. 2a). The corresponding elemental mapping images (Fig. 2b–e) show the homogeneous dispersion of Ti, C, O, and N elements throughout the nanosphere, further indicating the interpenetrating hetero-structure consists of NC and mTiO$_2$. The energy-dispersive X-ray spectrum (EDS) of the resultant NC/mTiO$_2$ nanospheres further confirms the coexistence of Ti, C, O, and N elements (Fig. 2f). These observations further demonstrate that titanium oligomers can work together with surfactants (HDA and P123) to form homogeneous hybrid frameworks during the self-assembly process. After annealing, the organic species transform into a continuous N-doped carbon framework throughout the highly crystallized TiO$_2$ matrix.
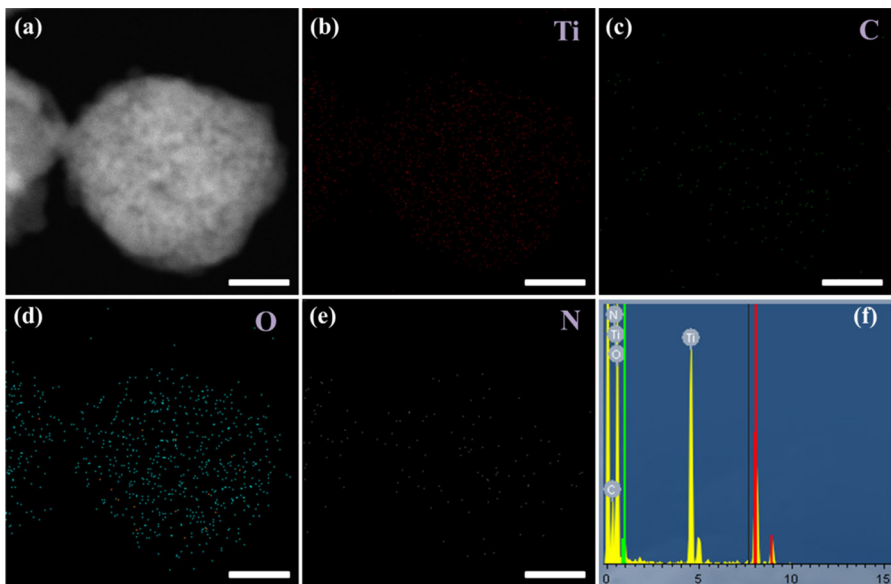

Fig. 2 **a** Scanning transmission electron microscopy (STEM) image, **b–e** corresponding elemental mapping images and **f** the energy-dispersive X-ray (EDX) analysis of Ti, C, O, and N elements for a NC/mTiO$_2$ composite nanosphere prepared via a sol–gel process followed by sequential carbonization of surfactants. All scale bars in TEM images are 20 nm

The XRD pattern of the NC/mTiO$_2$ composites reveals the characteristic peaks, which clearly confirms the anatase TiO$_2$. The crystal size in the resultant nanospheres can be calculated to be about 8.2 nm based on Scherrer's formula (Fig. 3a). The XPS analysis indicates the presence of C (285 eV) and N (399 eV) elements (Fig. 3b). The result can prove that the surfactants could be well transformed into NC through the carbonization approach, which can be further confirmed by the Raman spectrum analysis. Figure 3c displays two typical peaks around 1354 and 1571 cm^{-1} for the D and G-band of carbon from template–carbonization, respectively. Moreover, I_D/I_G value was calculated as ~ 1.61, suggesting a high degree of graphitization. Thermogravimetric analysis (TGA) discloses that the content of NC in NC/mTiO$_2$ is 2.2 wt% (Figure S3). The N$_2$ adsorption/desorption isotherms of the NC/mTiO$_2$ composite nanospheres show type IV curves (Fig. 3d), which suggest mesoporous characteristics [32]. The specific surface area is calculated to be as large as ~ 108 m^2/g. The pore size calculated by the Barrett–Joyner–Halenda (BJH) method using the adsorption branch is ~ 2.1 nm (Fig. 3d, inset), which is consistent with the SEM and TEM results.
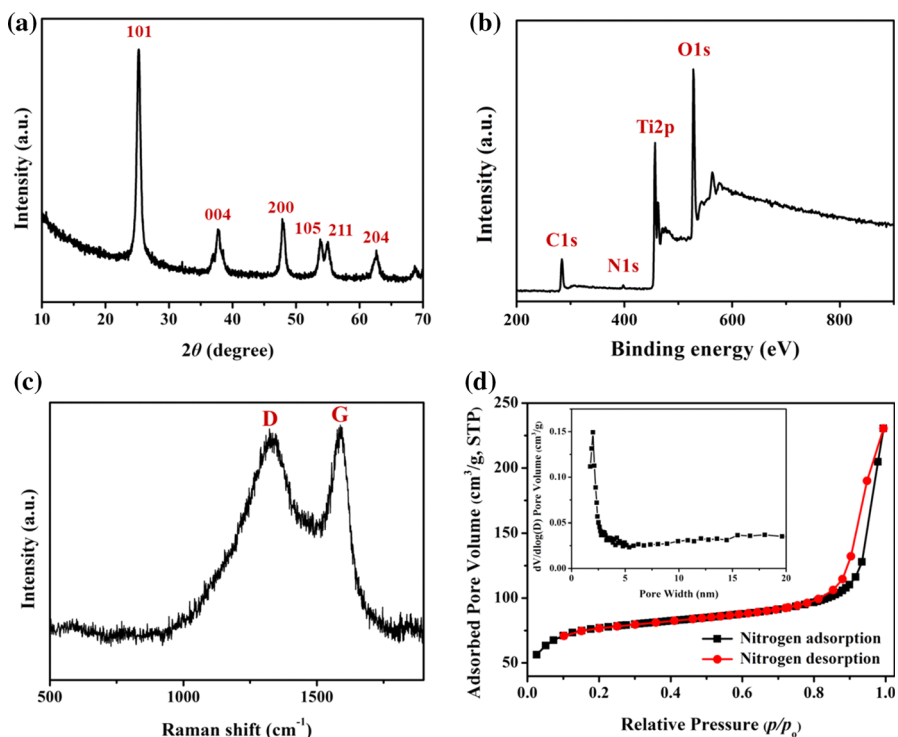

Fig. 3 a Wide-angle XRD pattern, b XPS survey spectrum, c Raman spectrum, and d nitrogen adsorption/desorption isotherms and the corresponding pore size distributions (inset) of NC/mTiO$_2$ composite nanospheres prepared via a sol–gel process followed by sequential carbonization of surfactants

The UV–Vis–NIR spectra (Figure S4) disclose that the NC/mTiO$_2$ composite nanospheres possess higher optical absorbance in an entire wavelength range (200–2000 nm) than commercial P25. The photocatalytic activity of the NC/mTiO$_2$ composite nanospheres was first verified by photodegradation of methyl orange. After photodegradation, methyl orange characteristic peaks shifted (Fig. 4a, c) and were significantly reduced with illumination time in a range from 10 to 180 min (Fig. 4d), indicating a high photodegradation of methyl orange. As shown in Fig. 4c, P25 has a low performance (19.8% within 180 min) in the UV–Vis light region. It is mainly because P25 almost has no activity in the visible light. Furthermore, when UV light is irradiated on the P25 surface, photogenerated electrons are excited to the conduction band (CB) but undergo a quick transition to the valence band (VB), thus leading to low quantum efficiency of TiO$_2$ [33]. In contrast, the resultant NC/mTiO$_2$ composite nanospheres showed much higher photocatalytic activity, and the methyl orange photodegradation efficiency reached 97.7% within 180 min. This excellent adsorption performance can be attributed to
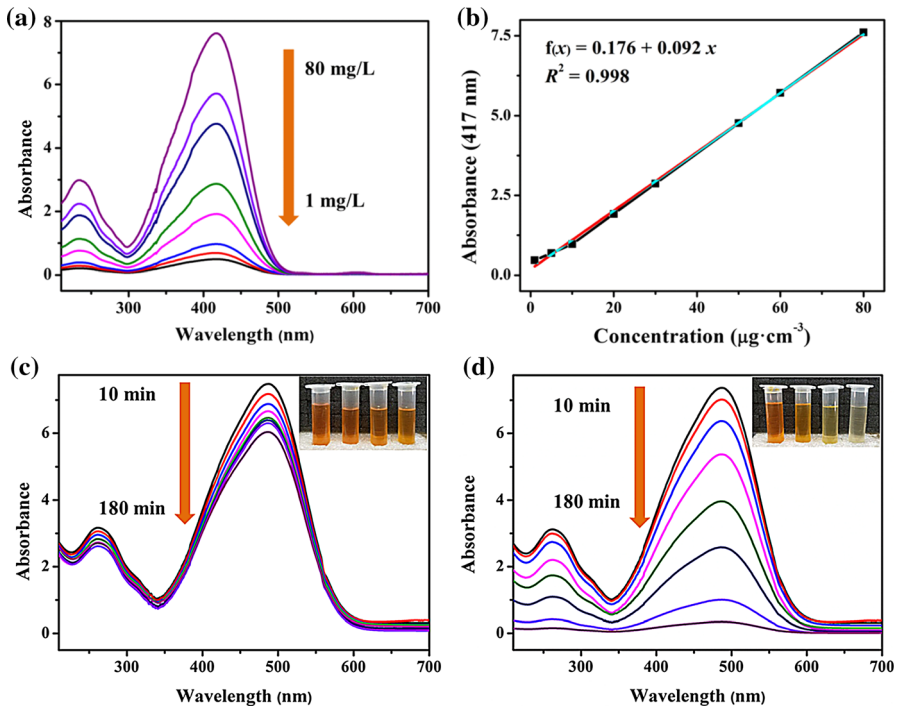

Fig. 4 **a** UV–Vis spectra of methyl orange solution in the range of 1–80 mg/L. **b** Linearization of the Bradford calibration graph for the absorbance at 417 nm in the range of 1–80 mg/L methyl orange solution. **c** UV–Vis spectra of the free methyl orange solution (80 mg/L, 50 mL) in the presence of commercial P25 (25 mg) under UV–Vis light irradiation (inset: optical image of the methyl orange solution with different time after the addition of commercial P25). **d** UV–Vis spectra of the free methyl orange solution (80 mg/L, 50 mL) in the presence of NC/mTiO$_2$ composite nanospheres (25 mg) under UV–Vis light irradiation (inset: optical image of the methyl orange solution with different time after the addition of NC/mTiO$_2$ composite nanospheres)

the following factors. Firstly, the NC with interpenetrating networks structure can prevent aggregation of ultrasmall TiO_2 nanocrystals ($\sim$ 8.2 nm) during the high-temperature treatment and photocatalytic operation, and the well-dispersed nanocrystals can greatly improve the photocatalytic activity (Fig. 5). Secondly, the large pore diameter (2.1 nm) can greatly facilitate the free diffusion and transportation of molecules to the inner surfaces, thus the high surface area ($\sim$ 108 m^2/g) can provide a sufficient space and surface active sites for photodegradation of organic pollutant molecules. Thirdly, the NC network possesses the strong adsorption ability for organic pollutant molecules (Fig. 5), and ensures repeated adsorption–catalysis processes [34, 35]. Fourthly, NC can enhance optical absorbance in the visible and NIR region and advance the photocatalytic activity [36, 37]. Fifthly, with the introduction of NC, a heterojunction forms at the interface, NCs can accept the photogenerated electrons from TiO_2, thus they hinder the electron–hole recombination and enhance the efficiency of photocatalytic oxidation (Fig. 5). In addtion, N-doping in the carbon matrix can greatly improve the electronic conductivity, thereby further improving the charge separation and photocatalytic efficiencies [33].

Moreover, the photodegradation experiments of other organic pollutants were also carried out, including dye and benzene derivatives. Figures 6 and 7 indicate that the photodegradation efficiency of 91.7 and 94.8% could be achieved after 180 min photocatalysis for methylene blue and phenol, respectively. The efficiencies are much higher than that of P25 (48.9 and 38.4% for methylene blue and phenol, respectively). These results suggest that the synthesized NC/mTiO$_2$
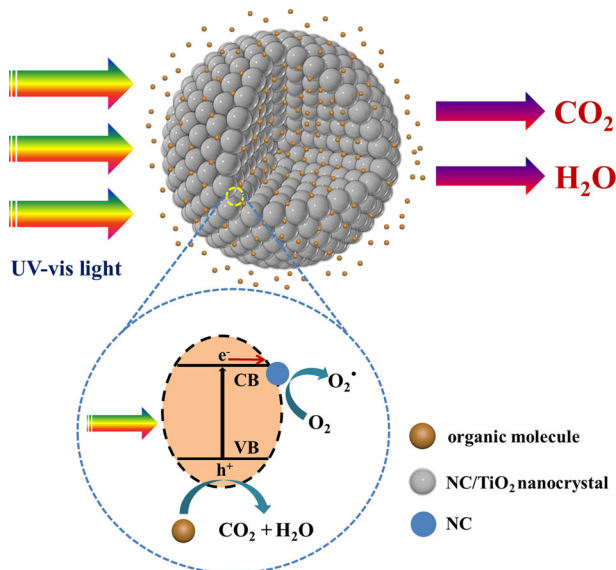

Fig. 5 Schematic illustration for photocatalysis of the NC/mTiO$_2$ composite nanospheres prepared via a sol–gel process followed by sequential carbonization of surfactants
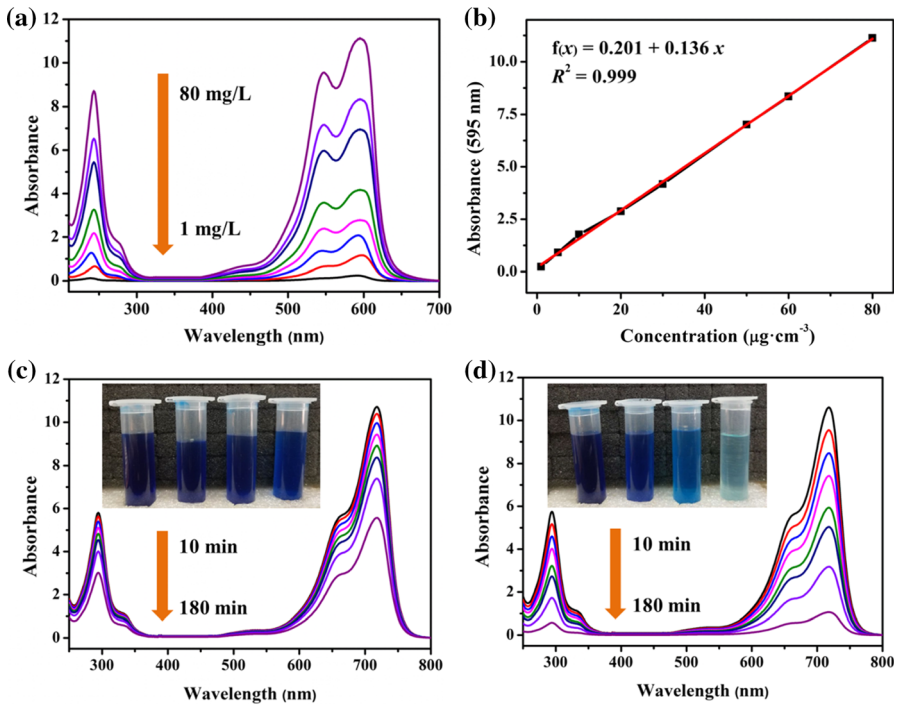
Fig. 6 **a** UV–Vis spectra of methylene blue solution in the range of 1–80 mg/L. **b** Linearization of the Bradford calibration graph for the absorbance at 595 nm in the range of 1–80 mg/L methylene blue solution. **c** UV–Vis spectra of the free methylene blue solution (80 mg/L, 50 mL) in the presence of P25 (25 mg) under UV–Vis light irradiation (inset: optical image of the methylene blue solution with different times after the addition of commercial P25). **d** UV–Vis spectra of the free methylene blue solution (80 mg/L, 50 mL) in the presence of NC/mTiO₂ composite nanospheres (25 mg) under UV–Vis light irradiation (inset: optical image of the methylene blue solution with different times after the addition of NC/mTiO₂ composite nanospheres)

composite nanospheres have the universality for multiple micropolluted water degradation.

Conclusions

In summary, we reported a versatile and simple method for the preparation of monodispersed NC/mTiO₂ composite nanospheres through a sol–gel process combined with an in situ carbonization strategy. In this case, homogeneous organic–inorganic frameworks were first formed during the self-assembly process. Then, the organic species could be directly transformed into a continuous N-doped carbon framework, which would effectively favor photogenerated electron transfer and separation of TiO₂. The NC/mTiO₂ nanocomposites possess a high surface area ($\sim$ 108 m²/g), large pore diameter (2.1 nm), and uniform particle size (60 nm), which consist of ultrasmall anatase TiO₂ nanocrystals ($\sim$ 8.2 nm). The resultant composite nanospheres exhibit superior photodegradation performance over a range
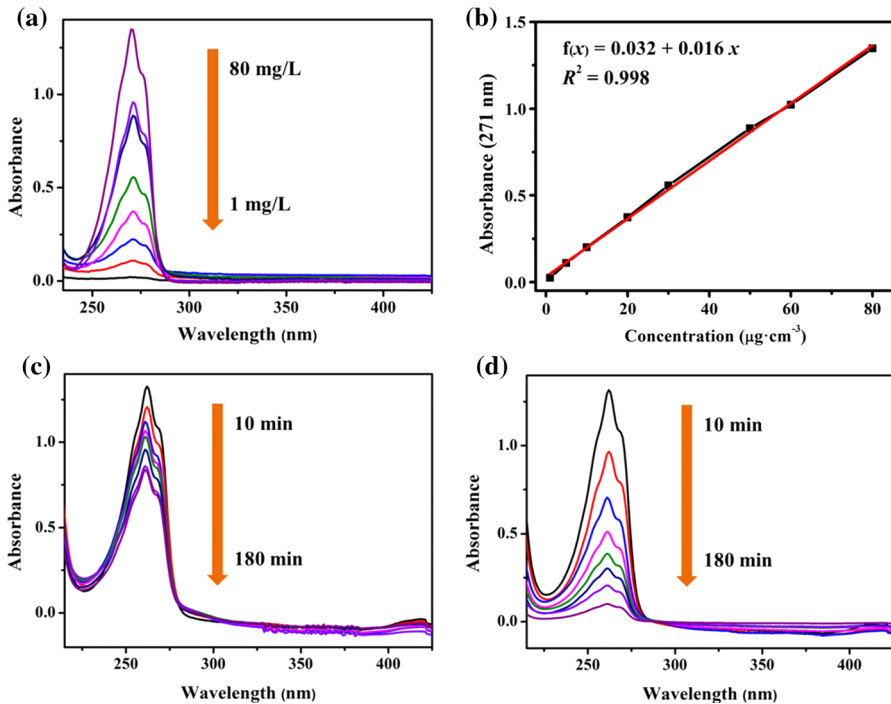
Fig. 7 a UV–Vis spectra of phenol solution in the range of 1–80 mg/L. **b** Linearization of the Bradford calibration graph for the absorbance at 271 nm in the range of 1–80 mg/L phenol solution. **c** UV–Vis spectra of the free phenol solution (80 mg/L, 50 mL) in the presence of P25 (25 mg) under UV–Vis light irradiation. **d** UV–Vis spectra of the free phenol solution (80 mg/L, 50 mL) in the presence of NC/mTiO$_2$ composite nanospheres (25 mg) under UV–Vis light irradiation

of organics such as methyl orange, methylene blue, and phenol compared to commercial P25 under the UV–Vis light irradiation. These results clearly indicate that NC/mTiO$_2$ nanocomposites are promising materials for the cleanup of organic pollutants in a natural water environment.

References

1. Y. Xu, T. Liu, Y. Zhang, F. Ge, R.M. Steel, L. Sun, J. Mater. Chem. A **5**, 12001 (2017)
2. A. Durán, J.M. Monteagudo, A. Carnicer, M. Ruiz-Murillo, Desalination **270**, 124 (2011)
3. S. Feng, X. Zhang, Y. Liu, Water Res. **86**, 35 (2015)
4. M. Magureanu, N.B. Mandache, V.I. Parvulescu, Water Res. **81**, 124 (2015)
5. T. Basile, A. Petrella, M. Petrella, G. Boghetich, V. Petruzzelli, S. Colasuonno, D. Petruzzelli, Ind. Eng. Chem. Res. **50**, 8389 (2011)
6. Y.P. Liu, J.C. Chen, W. Li, D.K. Shen, Y.J. Zhao, M. Pal, H.J. Yu, B. Tu, D.Y. Zhao, J. Colloid Interface Sci. **477**, 54 (2016)

7. J.M. Ochando-Pulido, S. Pimentel-Moral, V. Verardo, A. Martinez-Ferez, Sep. Purif. Technol. **179**, 161 (2017)
8. O. Sacco, V. Vaiano, C. Daniel, W. Navarra, V. Venditto, Mat. Sci. Semicon. Proc. **80**, 104 (2018)
9. W. Li, Q. Yue, Y.H. Deng, D.Y. Zhao, Adv. Mater. **25**, 5129 (2013)
10. Z.A.M. Hir, P. Moradihamedani, A.H. Abdullah, M.A. Mohamed, Mat. Sci. Semicon. Proc. **57**, 157 (2017)
11. R.K. Ibrahim, M. Hayyan, M.A. AlSaadi, A. Hayyan, S. Ibrahim, Environ. Sci. Pollut. Res. **23**, 13754 (2016)
12. H. Fakhri, A.R. Mahjoub, A.H. Cheshme Khavar, Mater. Sci. Semicon. Proc. **41**, 38 (2016)
13. W. Li, F. Wang, Y.P. Liu, J. Wang, J. Yang, L. Zhang, A.A. Elzatahry, D. Al-Dahyan, Y.Y. Xia, D.Y. Zhao, Nano Lett. **15**, 2186 (2015)
14. J. Yang, C. Hu, Y. Jin, H. Chen, W. Zhu, X. Zhou, Res. Chem. Intermed. (2018). https://doi.org/10.1007/s11164-018-3449-2
15. M. Zhang, Y. Fang, Y. Zhao, Z. Wang, L. Shi, J. Zhang, S. Yuan, Res. Chem. Intermed. **44**, 3017 (2018)
16. G. Gyawali, J. Son, N.H. Hao, S.H. Cho, T.H. Kim, S.W. Lee, Res. Chem. Intermed. **43**, 5055 (2017)
17. W. Li, J. Liu, D.Y. Zhao, Nat. Rev. Mater. **1**, 16023 (2016)
18. N.A. Almeida, P.M. Martins, S. Teixeira, J.A.L.D. Silva, V. Sencadas, K.K. Hn, G. Cuniberti, S. Lanceros-Mendez, P.A.A.P. Marques, J. Mater. Sci. **51**, 6974 (2016)
19. Y. Gao, M. Hu, B. Mi, J. Membr. Sci. **455**, 349 (2014)
20. J. Ren, X. Zhang, D. Lu, B. Chang, J. Lin, S. Han, Res. Chem. Intermed. (2018). https://doi.org/10.1007/s11164-018-3414-0
21. S.D. Perera, R.G. Mariano, K. Vu, N. Nour, O. Seitz, Y. Chabal Jr., K.J. Balkus, Catalysis **2**, 949 (2012)
22. A. Trapalisa, N. Todorova, T. Giannakopoulou, N. Boukos, T. Speliotis, D. Dimotikali, J. Yu, Appl. Catal. B **180**, 637 (2016)
23. Z. Mou, Y. Wu, J. Sun, P. Yang, Y. Du, A.C. Lu, ACS Appl. Mater. Interfaces **6**, 13798 (2014)
24. M.S.A.S. Shah, W.J. Kim, J. Park, D.K. Rhee, I. Jang, N. Park, J.Y. Lee, P.J. Yoo, ACS Appl. Mater. Interfaces **6**, 20819 (2014)
25. L. Qu, Y. Liu, J. Baek, L. Dai, ACS Nano **4**, 1321 (2010)
26. Y. Liu, F. Pei, R. Lu, S. Xu, S. Cao, Mater. Res. Bull. **60**, 188 (2014)
27. H. Xu, M. Ding, W. Chen, Y. Li, K. Wang, Sep. Purif. Technol. **195**, 70 (2018)
28. H.W. Zhu, Y. Jing, M. Pal, Y. Liu, Y. Liu, J. Wang, F. Zhang, D.Y. Zhao, Nanoscale **9**, 1539 (2017)
29. M. Mahyari, J.N. Gavgani, Res. Chem. Intermed. **44**, 3641 (2018)
30. D.H. Chen, L. Cao, F.Z. Huang, P. Imperia, Y.B. Cheng, R.A. Caruso, J. Am. Chem. Soc. **132**, 4438 (2010)
31. E.L. Crepaldi, G.J.A.A. Soler-Illia, D. Grosso, F. Cagnol, F. Ribot, C. Sanchez, J. Am. Chem. Soc. **125**, 9770 (2003)
32. Y.P. Liu, W. Li, D.K. Shen, C. Wang, X.M. Li, M. Pal, R.Y. Zhang, L. Chen, C. Yao, Y. Wei, Y.H. Li, Y.J. Zhao, H.W. Zhu, W.X. Wang, A.M. El-Toni, F. Zhang, D.Y. Zhao, Chem. Mater. **27**, 5577 (2015)
33. Z. Mou, Y. Wu, J. Sun, P. Yang, Y. Du, C. Lu, ACS Appl. Mater. Interfaces **6**, 13798 (2014)
34. W. Teng, Z. Wu, J. Fan, H. Chen, D. Feng, Y. Lv, J. Wang, A.M. Asirid, D.Y. Zhao, Energy Environ. Sci. **6**, 2765 (2013)
35. W. Teng, Z. Wu, J. Fan, W.X. Zhang, D.Y. Zhao, J. Mater. Chem. A **3**, 19168 (2015)
36. S.M. Chaudhari, P.M. Gawal, P.K. Sane, S.M. Sontakke, P.R. Nemade, Res. Chem. Intermed. **44**, 3115 (2018)
37. W. Zhang, Y. Zhou, C. Dong, B. Shen, M. Xing, J. Zhang, Res. Chem. Intermed. (2018). https://doi.org/10.1007/s11164-018-3269-4

Affiliations

Dian Li[1] · Yupu Liu[2] · Hong Liu[1] · Zhihua Li[1] · Li Lu[1] · Jun Liang[1] ·
Zhonghui Huang[1] · Wei Li[2] (iD)

[1]   Technical Center of China Tobacco Guangxi Industrial Co., Ltd, Nanning 530001, Guangxi,
       People's Republic of China

[2]   Department of Chemistry, Fudan University, Shanghai 200433, People's Republic of China